SLAC-PUB-815
April 1971
(TH) and (EXP)

INELASTIC ELECTRON-PROTON SCATTERING AT LARGE MOMENTUM TRANSFERS

G. Miller, E. D. Bloom, G. Buschhorn,* D. H. Coward,
H. DeStaebler, J. Drees,** C. L. Jordan, L. W. Mo,*** R. E. Taylor

Stanford Linear Accelerator Center†
Stanford University, Stanford, California 94305

J. I. Friedman, G. C. Hartmann,†† H. W. Kendall, R. Verdier

Physics Department and Laboratory for Nuclear Science†††
Massachusetts Institute of Technology, Cambridge, Massachusetts 02139

ABSTRACT

Differential cross sections for electrons scattered inelastically from hydrogen were measured at 18°, 26°, and 34°. The range of incident energy was 4.5 to 18 GeV, and the range of four momentum transfer squared was 1.5 to 21 $(\mathrm{GeV}/c)^2$. With the use of these data in conjunction with previously measured data at 6° and 10°, the contributions from the longitudinal and transverse components of the exchanged photon have been separately determined. The values of the ratio of the photoabsorption cross sections σ_S/σ_T were in the range 0 to 0.5.

(Submitted to Phys. Rev. Letters.)

---

* Present address: DESY, Hamburg, Germany.

** Present address: Bonn University, Bonn, Germany.

*** Present address: Department of Physics and the Enrico Fermi Institute, University of Chicago, Chicago, Illinois.

† Work supported by the U. S. Atomic Energy Commission.

†† Present address: Xerox Corporation, Rochester, New York.

††† Work supported in part by the U. S. Atomic Energy Commission under Contract No. AT(30-1)2098.

The measurements we report here extend our earlier study of inelastic electron-proton scattering at forward angles[1] to larger angles (θ), higher four-momentum transfer squared (q^2), and higher electron energy loss (ν) and allow a separation of the two electromagnetic structure functions of the proton. This paper presents the results of the separation; a discussion of the q^2 behavior of these functions and the implications of the measurements with regard to the question of scaling will be given in a second communication.[2] The differential cross sections $d^2\sigma/d\Omega dE'$ for inelastic electron-proton scattering have been measured at the Stanford Linear Accelerator Center by detecting the scattered electron at laboratory angles of 18°, 26° and 34°. Measurements were made at incident energies between 4.5 GeV and 18 GeV and at scattered electron momenta between the limit set by elastic scattering kinematics and 2 GeV/c, 1.75 GeV/c and 1.5 GeV/c respectively for the three angles. These measurements have been combined with our earlier measurements at 6° and 10° to provide a separation for various values of q^2 in the range from 1.5 to 11.0 $(GeV/c)^2$ over a range of W, from 2.0 to 4.0 GeV, where W is the mass of unobserved hadronic state.

In making the separation we have found it convenient to use the representation for the differential cross section employing the absorption cross sections, σ_T and σ_S, for virtual photons with transverse and longitudinal polarization components respectively.[3] On the assumption of one-photon exchange, the differential cross section in the laboratory frame can be written as follows[4]:

$$\frac{d^2\sigma(\theta, E, E')}{d\Omega dE'} = \Gamma_T \left(\sigma_T(q^2, W^2) + \epsilon \sigma_S(q^2, W^2)\right) \qquad (1)$$

$$\Gamma_T = \frac{\alpha}{4\pi^2} \frac{K}{q^2} \frac{E'}{E} \left(\frac{2}{1-\epsilon}\right)$$

$$\epsilon = \frac{1}{\left(1 + 2(1+\nu^2/q^2) \tan^2 \frac{\theta}{2}\right)} ; \quad 0 \leq \epsilon \leq 1 \ .$$

The quantity $K = \left(W^2 - M_p^2\right)/2M_p$, where M_p is the rest mass of the proton, $\nu = E-E'$, and $q^2 = 4EE' \sin^2 \theta/2$, E is the incident electron energy, and E' is the scattered energy. The measurements were taken over a large region of q^2, W^2 space as shown in Fig. 1, in order to provide a sufficiently fine grid of data so that the unfolding of radiative effects could be accomplished in a model-insensitive way. Radiatively corrected cross sections at constant values of q^2 and W^2 for different values of ϵ (which corresponds to different values of θ) allow the separate determination of σ_T and σ_S, which yields R, defined as σ_S/σ_T.

The following is a description of the experimental equipment and technique used to extract these results, with emphasis placed on modifications and problems specific to this experiment. The incident electron beam was typically defined in energy to $\Delta E/E = \pm 0.5\%$, and was focussed to a spot approximately 3 mm high and 6 mm wide. The incident beam position and angle, monitored continuously throughout the experiment, remained constant to $\pm$ 1 mm and ± 0.1 mrad, respectively. The number of incident electrons was measured to an absolute accuracy of $\pm$ 0.5% by two toroidal beam monitors which were intercalibrated with a Faraday cup several times during the experiment. Collimation studies of the incident beam were made to eliminate the possibility of a low energy, large area beam halo which could introduce systematic errors in the data taken at low secondary momenta.

The liquid hydrogen target was specially designed to handle the very large beam intensities used in this experiment. These were as high as 50 mA, in a 1.6 μsec beam pulse, at repetition rates up to 360 times per second. The condensing target contained a pump which recirculated the liquid hydrogen in a closed loop from the target cell through a heat exchanger in contact with a liquid hydrogen

reservoir. Extensive tests showed that the recirculation eliminated variations of target density with variations of electron beam cross-sectional area and intensity, to an accuracy of 2% in the scattering cross section. In addition, the density was shown to be constant within ± 1% throughout the actual experiment by detecting with the SLAC 1.6 GeV/c spectrometer protons recoiling elastically from the target. The density of the liquid hydrogen was 0.070 g/cm^3, determined from the temperature of the hydrogen measured by two hydrogen cryometers inserted in the target above and below the beam line. The 7-cm diameter target cell was an aluminum cylinder with .003 inch thick walls. The wall contribution to the scattering was measured by using an identical, but empty, aluminum cylinder mounted directly below the target assembly. Scattering from the replica target and other windows was typically 10% of the full target rate.

The scattered particles were momentum analyzed by the SLAC 8 GeV spectrometer.[5] The spectrometer focuses point-to-point and disperses momentum in the vertical plane, and focuses line-to-point and disperses the horizontal scattering angle in the horizontal plane. The magnets were calibrated to the same standard shunt as the magnets defining the incident beam energy. The alignments of the magnetic elements were frequently monitored during the experiment. All observed misalignments were such as change a ray by less than one-fifth of the designed resolution. In order to calculate the acceptance of the spectrometer, a model was derived that reproduced optics measurements obtained by directing the incident beam into the spectrometer and mapping out the acceptance with a large family of rays of various energies and angles. The momentum dispersion was approximately 3 cm/%, and the horizontal projected angle dispersion was approximately 4.5 cm/mrad. The vertical projected angle acceptance,

approximately 60 mrad, was determined by lead masks located before the last quadrupole magnet. The total acceptance of the spectrometer $\Delta\Omega(\Delta p/p)$ was 25.4 $(\text{mrad})^2$. This was calculated analytically and by a Monte Carlo method. The calculations agreed to ± 1%.

Particle detection, identification and angle-momentum measurements were accomplished by a system of detectors consisting in sequence of a threshold gas Cerenkov counter (C), a large plastic scintillation counter for triggering purposes, a scintillation counter hodoscope of 55 horizontal elements, a scintillation counter hodoscope of 41 vertical elements, another large trigger counter, a telescope of three scintillation counters preceded by one radiation length of lead (DEX), and a total absorption, lead-lucite shower counter (TA).

The two orthogonal hodoscopes defined the resolution of the spectrometer to ± 0.05% in momentum and ± 0.15 mrad in horizontal scattering angle. A restricted set of these hodoscope counters was used to define a smaller acceptance to investigate possible effects due to scattering from lead that masked the hodoscopes. Average cross sections calculated with the total acceptance and with the restricted acceptance agreed to 1% in the case where the cross sections were not strongly varying with momentum. The calculations of the acceptance were considered accurate to ± 2%.

An on-line computer system, utilizing an SDS 9300 computer, scanned the hodoscope buffers after each event, the charge monitors and six analog-to-digital converters. This information was written on magnetic tape for later analysis. A continuously updated cross section as well as updated detector efficiencies and inefficiencies due to hodoscope multiple tracks were evaluated on-line using a fraction of the events written on tape. The largest instantaneous counting rates occurred in the large trigger counters and were kept less than 5 per machine

pulse by regulating the incident beam intensity. The fast electronic dead times effects were less than 1%. The number of events per pulse was kept at rates less than 0.3 events per pulse.

The electron yields and cross sections for a particular E, E', θ setting, target type, and spectrometer polarity were calculated by counting the number of events on the data tape satisfying three different requirements, allowing successively greater electron-pion discrimination. The discrimination requirements were: (a) a large pulse height from the TA counter corresponding to a 99% efficiency for a pure electron sample; (b) a signal from the Cerenkov counter plus requirement (a); and (c) large pulse heights from all three DEX scintillation counters plus condition (b). Where the three cross sections agreed the least restrictive requirement having the largest number of successful events was used. All events were required to have good signals from both trigger scintillation counters and to represent particles unambiguously passing through the restricted set of hodoscope counters.

Discrimination of electrons from pions became a problem at the lowest secondary energies. The largest pion to electron ratio encountered was 300:1 where the pion rejection of the combined system (C)(DEX)(TA) was about 2×10^4:1, and the electron efficiency was 0.72. This low efficiency was due to the DEX system which had an energy dependent efficiency for electrons that ranged from 0.74 at 2 GeV to 0.88 at 8 GeV and had an uncertainty of $\pm$ 1.5%. For most points, DEX was not used, and the electron efficiency was 0.97. The error due to pion contamination was $\leq$ 2%.

Corrections were made for the electron detection efficiency of all counters, for the computer logging deadtime (less than 15%) and for ambiguous hodoscope bit patterns (typically 7%). The final measured cross section was corrected by subtracting the cross section for electrons scattered from the target walls and

the contribution from electrons coming from π^o decay and pair production, which was measured by reversing the polarity of the spectrometer and was negligible over most of the spectra except at the lowest scattered energies where it was always less than 25%.

The measured cross sections were corrected for radiative effects in the following way. First, the elastic radiative tail was subtracted. This was calculated using the formula of Tsai[6] for electron bremsstrahlung during the elastic scattering which is exact to lowest order in α. Radiative energy degradation of the incident and final electrons by the surrounding target material was also included along with corrections[7] for multiple photon effects and radiation from the recoiling proton. After the subtraction of the elastic tail, the inelastic radiative effects were removed in an unfolding procedure using a peaking-factorization approximation which allowed the radiative tail to be expressed as the sum of two one-dimensional integrals involving the previously corrected cross sections at the same angle. The particular version of the peaking-factorization approximation used was determined by a direct comparison with an exact calculation of the inelastic radiative tail, assuming a model which approximated the experimentally determined inelastic form factors.

The inelastic radiative tail corrections were assigned an error of ± 10% to take into account both the inaccuracy of the peaking approximation and errors introduced by interpolation of the cross section. The different methods of interpolation used changed the corrected cross sections by less than half of the statistical error. The elastic tail corrections were assigned an average error of ± 3% which reflect uncertainties as large as 5%. The maximum total radiative correction was 30%, and the corrections were generally smaller than those at the lower angles.[1]

Elastic e-p scattering was measured for nine combinations of incident energy and scattering angle, and two different analyses were done. First, the effects of radiation were unfolded using a method described in another publication.[8] Secondly, the theoretical cross section was folded with radiation effects, the incident energy spectrum, and the spectrometer resolution using the elastic form factors previously reported by the MIT-SLAC collaboration[9] together with the elastic scattering measurements taken at 6^{o} and 10^{o} with the 20 GeV spectrometer. Both methods gave similar results that indicated that the apparatus had no systematic errors comparable to the statistical errors of approximately 3%. This result is especially important for those separations of σ_T and σ_S that also rely on data taken at small angles with the 20 GeV spectrometer. Typically, a systematic 3% difference between the 6^{o} and 10^{o} data and the present data would change the ratio $R = \sigma_S/\sigma_T$ by 0.06. This uncertainty is small compared to the statistical errors in the values of R.

Figure 2 shows the radiatively corrected spectrum for E = 18 GeV, and $\theta = 26^{o}$ along with the radiative correction factor, defined as the ratio of the final corrected cross section to the measured cross section.

Table I gives the values of the radiatively corrected cross sections for which $W \geq 1.8$ GeV. The quoted errors reflect both counting statistics and parts of other estimated uncertainties two of which are the errors described above for the elastic and inelastic radiative tails. Not included is an additional overall systematic error that is estimated to be ± 5%.

The shaded area of the $q^2 - W^2$ plane in Fig. 1 shows the kinematic range over which σ_S and σ_T can be separated, requiring data at a minimum of three values of ϵ. Actual data points at different angles for the same values of q^2 and W^2 exist only for $q^2 = 4(\text{GeV/c})^2$; W=2, 3, and 4 GeV. However, the data at

each angle are sufficiently finely spaced that they can be reliably interpolated to a particular point in the q^2, W^2 plane. Separations with several different interpolation methods indicated that the results were insensitive to the particular procedure used. Twenty points (q^2, W^2) were chosen to represent the actual amount of data taken, some emphasis being placed on those areas with data at four or more values of ϵ. Figure 3 shows four examples of ϵ-plots used to obtain these ratios. The assumption of one photon exchange which underlies the definition of the electromagnetic structure functions, implies a linear dependence of $(d^2\sigma/d\Omega dE')/\Gamma_T$ on ϵ for a particular point (q^2, W^2). The data are everywhere consistent with this requirement.

Table II gives the 23 values of R, σ_T and σ_S along with their estimated random errors. The errors in R take account of the correlation between σ_S and σ_T. The R values are in the range 0 to 0.5, and no striking kinematic variation is apparent. In addition to the random errors quoted, we estimate that there are systematic errors that might change the values of R by $\pm$ 0.06.

On the assumption that R is a constant in this kinematic range, we find that for this particular set of points the average value of R = 0.18 $\pm$ 0.10, where the above mentioned systematic error is included linearly. The values of R obtained are also compatible with $R = aq^2$, with $a \approx 0.035$ $(GeV/c)^{-2}$, and with $R \approx q^2/\nu^2$. These two forms are suggested by theoretical considerations.[10] Undoubtedly, various other forms would also be compatible with our results.

The results of our separation of σ_T and σ_S show that σ_T is dominant in the kinematic region that we have investigated. The smallness of R precludes a definite statement that σ_S is significantly different from zero. The lack of measurements in the region $2M_p\nu/q^2 > 10$ prohibits a comparison with some diffractive models for R, but we find that R is small for values of $2M_p\nu/q^2$ up to about 8 and is not varying strongly with kinematics.

The group wishes to thank Professor W.K.H. Panofsky, the Spectrometer Facilities Group, and the Technical Division under R. B. Neal for their support in this project.

REFERENCES

1. E. D. Bloom et al., Phys. Rev. Letters 23, 930 (1969).

2. Submitted for publication in Phys. Rev. Letters.

3. L. Hand, Ph.D. dissertation, Stanford University (1961) and Phys. Rev. 129, 1834 (1963).

4. The differential cross section can be expressed in terms of two structure functions W_1 and W_2 such that

$$\frac{d^2\sigma}{d\Omega dE'} = \frac{4\alpha^2(E')^2}{q^4}\left[W_2(q^2,W^2)\cos^2\frac{\theta}{2} + 2W_1(q^2,W^2)\sin^2\frac{\theta}{2}\right]$$

These structure functions are related to the two absorption cross sections for virtual photons in the following way

$$W_2 = \frac{K}{4\pi^2\alpha}\left(\frac{q^2}{q^2+\nu^2}\right)(\sigma_T+\sigma_S)$$

$$W_1 = \frac{K}{4\pi^2\alpha}\,\sigma_T$$

A detailed discussion of these quantities is given, for example, by F. Gilman, Phys. Rev. 167, 1365 (1968).

5. R. E. Taylor, International Symposium on Electron and Photon Interactions at High Energies, Stanford Linear Accelerator Center (1967).

6. L. W. Mo and Y. S. Tsai, Rev. Mod Phys. 41, 205 (1969).

7. Guthrie Miller, Ph.D. dissertation, Stanford University (1970), Report No. SLAC-129. The appendix contains the exact statement of the formulas used to radiatively correct these data. Multiple photon corrections are different from Ref. 6.

8. P. N. Kirk et al., to be submitted to Phys. Rev.

9. D. H. Coward et al., Phys. Rev. Letters 20, 292 (1969).

10. The kinematic dependence $R = aq^2$, where a is a constant, is compatible with the gauge invariance requirement that $\sigma_S = 0$ at $q^2 = 0$. The relation $R = q^2/\nu^2$ would hold if, in the laboratory frame,

$$\sum_A \left| \langle A | j_{\parallel}^{\gamma} | p \rangle \right|^2 = \sum_A \left| \langle A | j_{\perp}^{\gamma} | p \rangle \right|^2$$

where p is the initial proton state, A is an arbitrary final state, $j_{\parallel}^{\gamma}$ and $j_{\perp}^{\gamma}$ are the longitudinal and transverse current operators respectively, and the sum is over all possible final states. Such behavior leads to the relation between the structure functions, W_1 and W_2, $\nu W_2 = (q^2/\nu) W_1$.

TABLE CAPTIONS

I. Radiatively corrected differential cross sections for inelastic electron-proton scattering. All measured points with $W \geq 1.8$ GeV are listed. The errors are approximately statistical standard deviations. An estimated overall systematic error of $\pm 5\%$ is not included.

II. $R, \sigma_T, \sigma_S, W_1$ and W_2 for 23 values of q^2 and W^2 using data taken at 6°, 10°, 18°, 26°, and 34°. The errors arise from the propagation of the errors given in Table I. The effects of overall systematic errors are not included. We estimate that systematic errors could make R uncertain by about $\pm .06$.

TABLE I

Radiatively Corrected Cross Sections for $W \geq 1.8$ GeV

θ (deg)	E (GeV)	E' (GeV)	$d^2\sigma/d\Omega dE'$ (10^{-35} cm^2/sr-GeV)
18	4.501	2.250	7600. ± 430.
		2.000	7000. ± 450.
	6.503	3.500	1879. ± 54.
		3.000	2413. ± 75.
		2.500	2593. ± 93.
		2.000	2510. ± 120.
	8.598	4.780	460. ± 15.
		4.500	572. ± 17.
		4.000	779. ± 44.
		3.500	957. ± 36.
		3.000	1036. ± 50.
		2.500	1229. ± 65.
		2.000	1330. ± 130.
	10.404	5.500	180.6 ± 6.3
		5.000	284. ± 10.
		4.500	409. ± 16.
		3.940	512. ± 23.
		3.500	604. ± 32.
		3.000	630. ± 40.
		2.500	751. ± 47.
		2.000	801. ± 99.
	13.299	7.000	19.88 ± .90
		6.500	49.2 ± 1.9
		6.000	93.0 ± 3.6
		5.500	135.8 ± 5.6
		5.000	178.2 ± 7.7
		4.500	208. ± 15.
		4.000	263. ± 21.
		3.500	306. ± 28.
		3.090	315. ± 23.
		2.500	417. ± 49.
		2.000	533. ± 74.
	17.000	8.000	7.08 ± .35
		7.500	15.17 ± .56
		7.000	29.9 ± 1.1
		6.500	44.8 ± 1.7
		6.000	64.3 ± 2.6
		5.500	86.9 ± 3.4
		5.000	101.1 ± 7.4
		4.500	122.8 ± 9.4
		4.000	145. ± 12.
		3.500	173. ± 16.
		3.000	191. ± 20.
		2.500	239. ± 31.
		2.000	271. ± 54.
26	4.494	2.000	1410. ± 67.
		1.800	1518. ± 81.
26	6.700	2.940	212.6 ± 7.8
		2.750	283.1 ± 10.
		2.500	340. ± 14.
		2.250	407. ± 19.
		2.000	504. ± 25.
		1.750	585. ± 51.
	8.696	3.750	32.2 ± 2.0
		3.500	57.2 ± 3.0
		3.250	91.7 ± 3.7
		3.000	119.9 ± 5.0
		2.750	154.9 ± 6.8
		2.500	195.5 ± 9.7
		2.270	229. ± 12.
		2.000	275. ± 17.
		1.750	317. ± 20.
	11.905	4.500	4.70 ± .48
		4.250	9.34 ± .99
		4.000	17.7 ± 1.0
		3.750	25.9 ± 1.6
		3.500	35.1 ± 2.2
		3.250	47.0 ± 4.5
		3.000	63.4 ± 6.2
		2.750	76.9 ± 7.7
		2.500	91.2 ± 9.9
		2.250	113. ± 12.
		2.000	121. ± 17.
		1.670	161. ± 23.
	15.006	5.000	1.34 ± .17
		4.750	2.87 ± .26
		4.500	5.55 ± .39
		4.250	8.07 ± .50
		4.000	13.83 ± .91
		3.750	18.4 ± 1.5
		3.500	23.3 ± 1.3
		3.250	31.6 ± 1.8
		3.000	39.6 ± 2.3
		2.750	45.9 ± 4.3
		2.500	52.0 ± 5.4
		2.250	62.7 ± 7.6
		2.000	76. ± 10.
		1.750	79. ± 15.
	18.030	5.500	.500 ± .090
		5.250	1.09 ± .15
		5.000	1.31 ± .20
		4.750	2.76 ± .29
		4.500	4.78 ± .39
		4.250	7.66 ± .55
		4.000	10.14 ± .99
26	18.030	3.750	12.9 ± 1.2
		3.500	15.3 ± 1.7
		3.250	21.5 ± 1.7
		3.000	25.7 ± 2.5
		2.750	32.9 ± 4.1
		2.500	39.4 ± 5.2
		2.250	45.7 ± 7.3
		2.000	56. ± 10.
		1.750	81. ± 16.
34	4.501	1.600	404. ± 22.
		1.400	533. ± 31.
		1.200	652. ± 41.
	5.795	2.020	108.0 ± 7.6
		1.750	175.3 ± 9.6
		1.500	252. ± 21.
		1.250	356. ± 33.
	7.899	2.500	24.8 ± 1.6
		2.250	38.2 ± 3.3
		2.000	62.4 ± 5.1
		1.750	90.4 ± 8.0
		1.480	125. ± 12.
		1.250	153. ± 21.
	9.999	3.000	3.02 ± .35
		2.750	8.60 ± .57
		2.500	15.03 ± .86
		2.250	26.1 ± 1.2
		2.000	36.4 ± 2.9
		1.750	47.2 ± 4.4
		1.500	70.3 ± 7.4
		1.250	104. ± 13.
	12.500	3.250	1.22 ± .19
		3.000	3.52 ± .40
		2.750	7.57 ± .55
		2.500	10.32 ± .64
		2.250	17.1 ± 1.7
		2.000	21.9 ± 2.4
		1.750	32.1 ± 4.0
		1.500	47.8 ± 6.6
		1.250	61. ± 13.
	14.996	3.250	0.85 ± .25
		3.000	2.29 ± .38
		2.750	4.30 ± .53
		2.500	7.21 ± .99
		2.250	11.8 ± 1.8
		2.000	16.7 ± 2.0
		1.750	19.6 ± 3.0
		1.500	32.6 ± 5.4

1687A44

TABLE II

q^2 $(GeV/c)^2$	W GeV	σ_T 10^{-30} cm^2	σ_S 10^{-30} cm^2	R	$2M_pW_1$	νW_2
1.5	2.0	42.8 ± 5.3	-2.8 ± 6.6	-.06 ± .15	1.19 ± .15	.290 ± .012
1.5	2.5	31.7 ± 3.3	4.8 ± 3.7	.15 ± .13	1.52 ± .16	.344 ± .005
1.5	3.0	26.7 ± 2.8	5.4 ± 3.3	.20 ± .14	1.93 ± .20	.343 ± .007
1.5	3.3	25.3 ± 2.8	5.8 ± 3.6	.23 ± .17	2.26 ± .25	.347 ± .011
3.0	2.0	16.1 ± 1.9	.75 ± 2.6	.05 ± .17	.45 ± .05	.179 ± .009
3.0	2.5	15.8 ± 1.5	2.0 ± 2.0	.12 ± .14	.76 ± .07	.265 ± .008
3.0	3.0	15.7 ± 1.6	1.7 ± 2.2	.11 ± .15	1.14 ± .11	.314 ± .014
3.0	3.4	13.3 ± 2.0	4.3 ± 2.8	.32 ± .26	1.27 ± .19	.349 ± .019
4.0	2.0	8.8 ± 1.3	2.0 ± 1.7	.23 ± .23	.244 ± .038	.131 ± .005
4.0	3.0	11.0 ± 1.2	2.0 ± 1.8	.18 ± .18	.799 ± .086	.284 ± .016
4.0	4.0	9.0 ± 1.7	4.5 ± 3.0	.50 ± .43	1.22 ± .23	.369 ± .039
5.0	2.0	5.82 ± .63	1.0 ± .9	.17 ± .17	.162 ± .018	.092 ± .004
5.0	2.5	7.38 ± .57	1.1 ± .8	.15 ± .12	.353 ± .027	.169 ± .005
5.0	3.0	8.23 ± .65	1.4 ± 1.0	.17 ± .13	.596 ± .047	.240 ± .009
5.0	3.4	8.0 ± 1.2	2.2 ± 1.8	.27 ± .27	.763 ± .113	.289 ± .019
8.0	2.0	1.82 ± .25	.58 ± .35	.32 ± .24	.051 ± .007	.039 ± .002
8.0	2.5	2.95 ± .27	.57 ± .41	.20 ± .16	.141 ± .013	.087 ± .004
8.0	3.0	3.55 ± .33	1.30 ± .59	.37 ± .20	.257 ± .024	.157 ± .009
8.0	3.5	4.15 ± .54	1.6 ± 1.1	.39 ± .30	.420 ± .055	.224 ± .021
8.0	4.0	4.99 ± .74	.3 ± 1.8	.06 ± .37	.67 ± .10	.235 ± .048
11.0	2.0	.74 ± .16	.34 ± .23	.46 ± .40	.021 ± .004	.020 ± .001
11.0	2.5	1.44 ± .18	.28 ± .28	.20 ± .22	.069 ± .008	.048 ± .003
11.0	3.0	1.82 ± .22	.89 ± .41	.49 ± .29	.132 ± .016	.102 ± .008

1687A45

FIGURE CAPTIONS

1. The regions of the kinematic $q^2 - W^2$ plane covered by the measurements at 18^o, 26^o and 34^o. The shaded area represents the region where data at 3 or more angles exist. Previously measured 6^o and 10^o data were also used in the separations.

2. (a) The radiatively corrected inelastic scattering spectrum $d^2\sigma/d\Omega dE'$ for E_0=18 GeV, θ=26^o. (b) The radiative correction applied to the data as a function of E', defined as the ratio of the final corrected cross section to the measured cross section.

3. Typical examples illustrating the separate determination of σ_S and σ_T. The straight solid lines are best fits to Eq. (1). The dashed lines indicate the one standard deviation values of the fits. The assumption of one-photon exchange made in calculating σ_S and σ_T implies that linear fits should be satisfactory. For the two upper graphs measured data exist at each angle. For the two lower graphs the data were interpolated. Effects of overall systematic errors are not included.

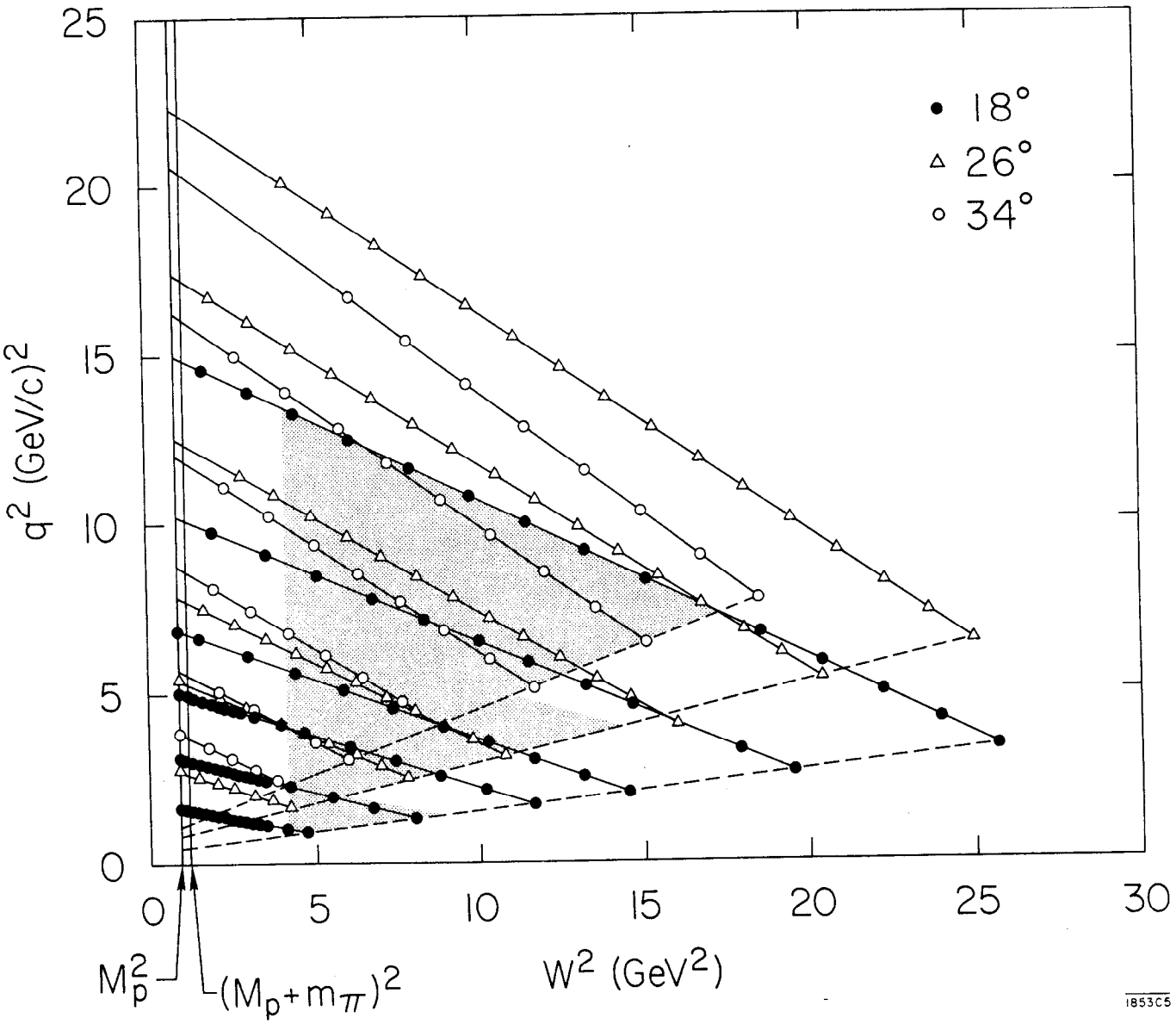
25
20
15
10
5
0
q^2 (GeV/c)^2
• 18°
△ 26°
○ 34°
0
5
10
15
20
25
30
W^2 (GeV^2)
M_p^2
$(M_p+m_\pi)^2$
1853C5

Fig. 1

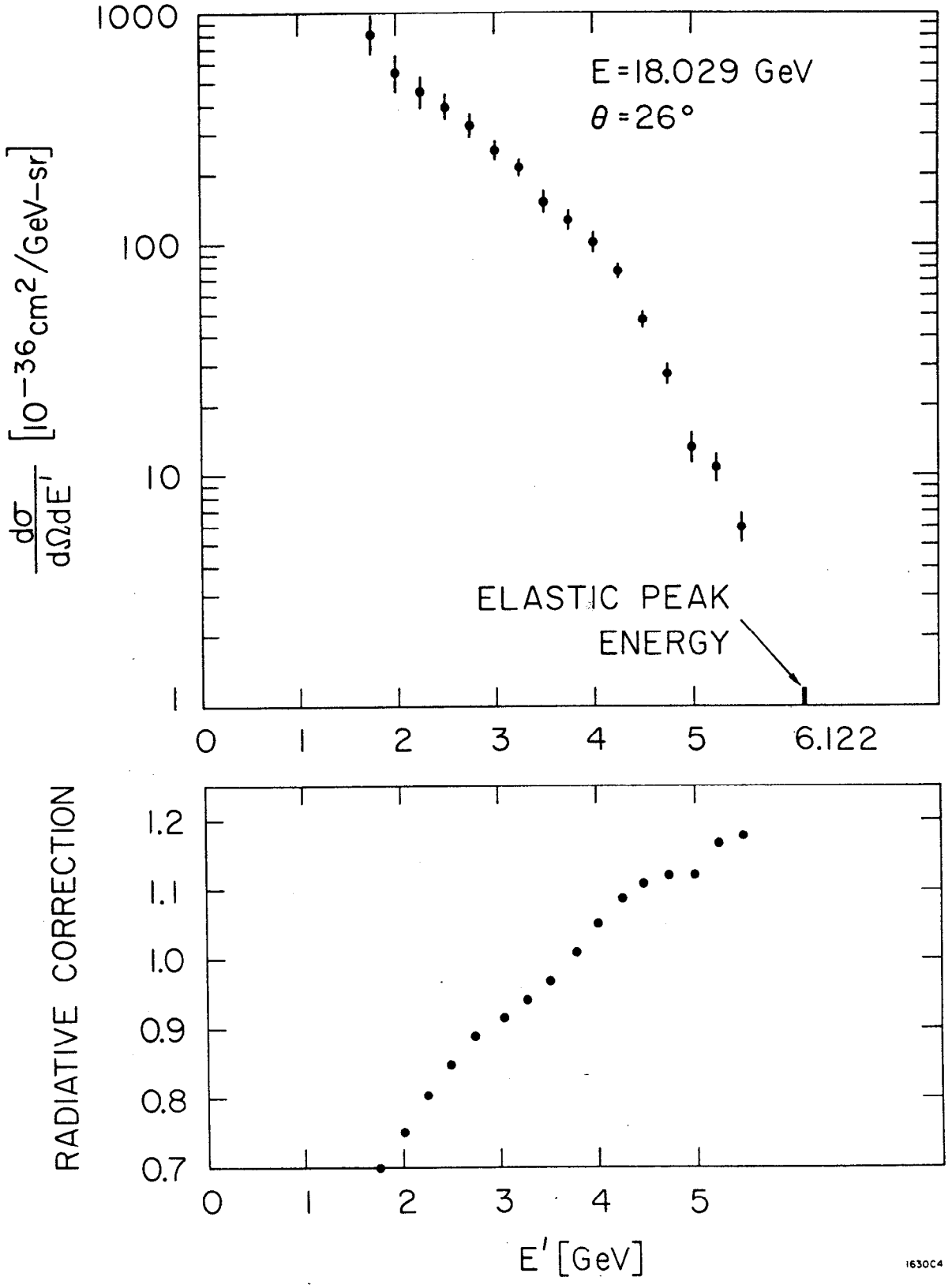
1000
100
10
1
E=18.029 GeV
θ=26°
ELASTIC PEAK
ENERGY
0
1
2
3
4
5
6.122
dσ/dΩdE' [10^-36 cm^2/GeV-sr]
RADIATIVE CORRECTION
1.2
1.1
1.0
0.9
0.8
0.7
E' [GeV]
1630C4

Fig. 2

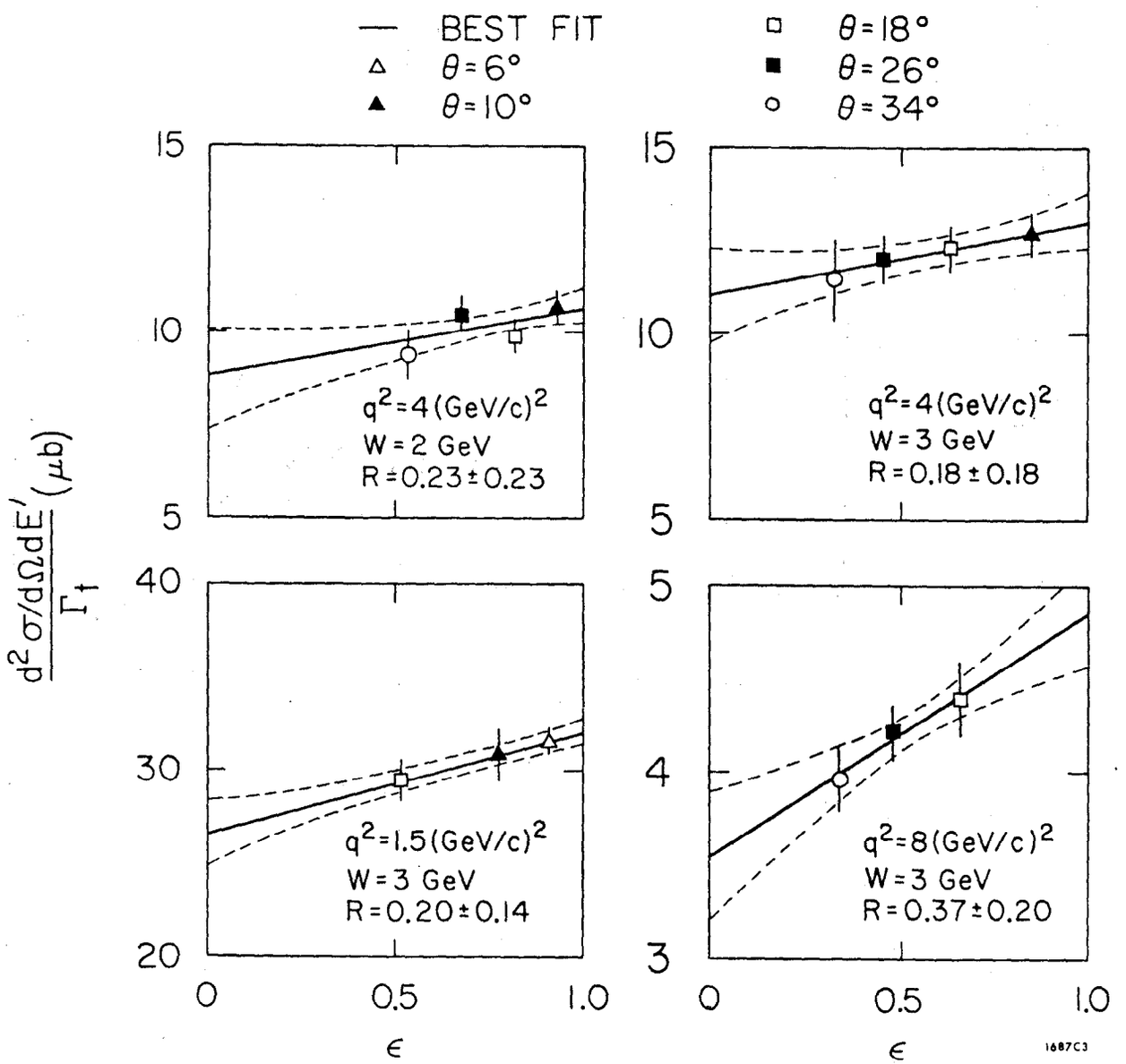
— BEST FIT
△ θ=6°
▲ θ=10°
□ θ=18°
■ θ=26°
○ θ=34°
$\frac{d^2\sigma/d\Omega dE'}{\Gamma_t}$ (μb)
q^2=4 (GeV/c)^2
W=2 GeV
R=0.23±0.23
q^2=4 (GeV/c)^2
W=3 GeV
R=0.18±0.18
q^2=1.5 (GeV/c)^2
W=3 GeV
R=0.20±0.14
q^2=8 (GeV/c)^2
W=3 GeV
R=0.37±0.20
ε
ε
1687C3

Fig. 3